Geometry-Adaptive Network for Robust Detection of Placenta Accreta Spectrum Disorders

Zailiang Chen[1], Jiang Zhu[1], Hailan Shen[1(✉)], Hui Liu[2], Yajing Li[1], Rongchang Zhao[1], and Feiyang Yu[1]

[1] School of Computer Science and Engineering, Central South University, Changsha, China
hn_shl@126.com

[2] Xiangya Hospital, Central South University, Changsha, China

Abstract. Placenta accreta spectrum (PAS) is a high-risk obstetric disorder associated with significant morbidity and mortality. Since the abnormal invasion usually occurs near the uteroplacental interface, there is a large geometry variation in the lesion bounding boxes, which considerably degrades the detection performance. In addition, due to the confounding visual representations of PAS, the diagnosis highly depends on the clinical experience of radiologists, which easily results in inaccurate bounding box annotations. In this paper, we propose a geometry-adaptive network for robust PAS detection. Specifically, to deal with the geometric prior missing problem, we design a Geometry-adaptive Label Assignment (GA-LA) strategy and a Geometry-adaptive RoI Fusion (GA-RF) module. The GA-LA strategy dynamically selects positive PAS candidates (RoIs) for each lesion according to its shape information. The GA-RF module aggregates the multi-scale RoI features based on the geometry distribution of proposals. Moreover, we develop a Lesion-aware Detection Head (LA-Head) to leverage high-quality predictions to iteratively refine inaccurate annotations with a novel multiple instance learning paradigm. Experimental results under both clean and noisy labels indicate that our method achieves state-of-the-art performance and demonstrate promising assistance for PAS diagnosis in clinical applications.

Keywords: PAS detection · Geometric information · Inaccurate annotations · Magnetic resonance imaging

1 Introduction

Placenta accreta spectrum (PAS) refers to the abnormal invasion of trophoblast cells into the myometrium at different depths of infiltration [10]. With the rising trend of advanced maternal age and cesarean section delivery, the incidence of PAS has increased steadily in recent years [5]. Undiagnosed PAS may lead to

H. Greenspan et al. (Eds.): MICCAI 2023, LNCS 14226, pp. 43–53, 2023.
https://doi.org/10.1007/978-3-031-43990-2_5

massive obstetric hemorrhage and hysterectomy [21]. Therefore, accurate detection of PAS prenatally is critical for appropriate treatment planning. Magnetic resonance imaging (MRI) provides valuable position information of placenta and can be an important complementary imaging method when ultrasound (US) diagnosis is inconclusive [1,15]. Since manually identifying PAS on MR images is time-consuming and labor-intensive, automated detection of PAS is significant in clinical practice.

However, due to the lack of open-source dataset, the research on computer-aided diagnosis of PAS is very limited. Previous studies [17,18,20,29] mainly focused on the classification task but accurate location cannot be provided. Moreover, existing object detection methods are designed for natural images [3,19,23,30] or specific diseases [16,22,27], with no consideration for the characteristics of PAS. Given that the abnormal invasion usually occurs near the uteroplacental interface, the geometric information of lesion regions is highly correlated with the shape of placenta, thereby causing significant variation in the aspect ratios of PAS bounding boxes. Furthermore, MRI in most cases is used after suspecting an abnormality on US, this by itself raises the difficulty of accurate labeling [19].

To address the above issues, we propose a novel geometry-adaptive PAS detection method, which utilizes the shape prior of placenta to predict high-quality PAS bounding boxes and further refines inaccurate annotations. The prior knowledge is mainly reflected in the aspect ratio of lesion boxes. Specifically, to take advantage of the geometry prior, we design a Geometry-adaptive Label Assignment (GA-LA) strategy and a Geometry-adaptive RoI Fusion (GA-RF) module. The GA-LA strategy dynamically selects positive proposals by calculating the optimal IoU threshold for each lesion. The GA-RF module fuses multi-scale RoI features from different pyramid layers. To reduce the impact of lesions with large aspect ratio, the module generates fusion weights through the geometry distribution of proposals. Furthermore, in order to alleviate the reliance on accurate annotations, we construct a Lesion-aware Detection Head (LA-Head), which leverages the geometry-guided predictions to iteratively refine bounding box labels by multiple instance learning. To the best of our knowledge, this is the first work to automatically detect PAS disorders on MR images. The contributions of this paper can be summarized as follows: (1) A Lesion-aware Detection Head (LA-Head) is designed, which employs a new multiple instance learning approach to improve the robustness to inaccurate annotations. (2) A flexible Geometry-adaptive Label Assignment (GA-LA) strategy is proposed to select positive PAS candidates according to the shape of lesions. (3) A statistic-based Geometry-adaptive RoI Fusion (GA-RF) module is developed for aggregating multi-scale features based on the geometry distribution of proposals.

2 Method

The central idea of our geometry-adaptive network is to refine inaccurate bounding boxes with geometry-guided predictions. To this end, we propose a Geometry-adaptive Label Assignment (GA-LA) strategy and a Geometry-adaptive RoI

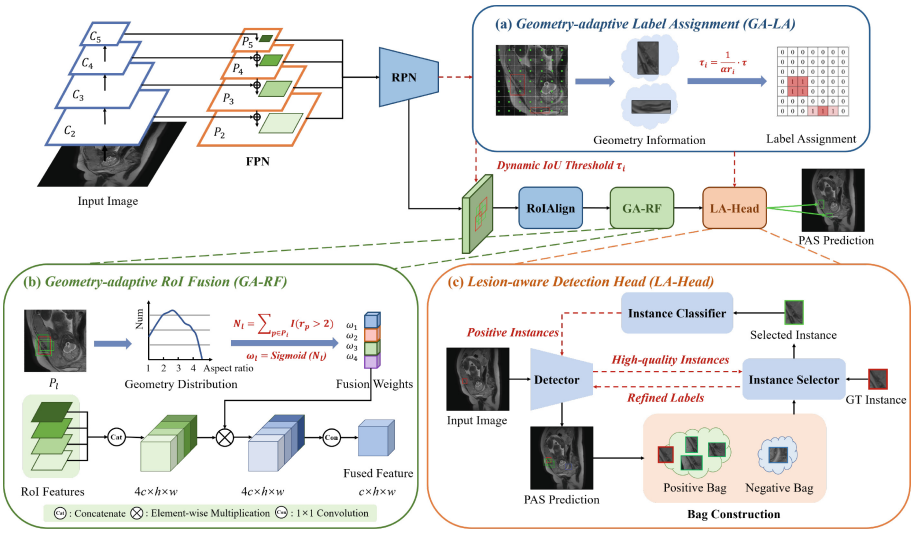

Fig. 1. Overview of our geometry-adaptive network, with novel (a) GA-LA, (b) GA-RF and (c) LA-Head. To solve the geometric prior missing problem, GA-LA strategy dynamically selects PAS RoIs according to the shape of placenta, and then GA-RF module fuses multi-scale features based on their geometry distribution. With the high-quality predictions, LA-Head refines inaccurate annotations by multiple instance learning.

Fusion (GA-RF) module to introduce geometry prior to detection. Then we develop a Lesion-aware Detection Head (LA-Head) to achieve the refinement of inaccurate annotations using multiple instance learning.

The overview of our method is illustrated in Fig. 1. Given an input image, Feature Pyramid Network (FPN) [12] extracts image features and then Region Proposal Network (RPN) [19] generates a set of region proposals. After obtaining the candidate boxes, RoIAlign [7] maps them to feature pyramid levels and extracts each proposal as a fixed-size feature map. Then the GA-RF module aggregates the multi-scale representations of each level through the statistical geometric information. Based on the fused RoI feature map, the LA-Head predicts and refines the classification and localization of lesions. During training, the GA-LA strategy assigns label to each proposal according to the shape of corresponding ground-truth box, making the model directly trainable.

2.1 Geometry-Adaptive Label Assignment

The static label assignment strategy adopted by Faster R-CNN predefines the IoU threshold τ to match objects and background to each anchor, but ignores the different shapes of PAS regions. To relieve the problem, we propose a GA-LA strategy to dynamically calculate the IoU threshold τ_i for each lesion bounding box g_i according to its aspect ratio r_i. A previous study demonstrated that

the aspect ratio is larger, the detection performance is better with a low IoU threshold [9,26]. Therefore, the value of τ_i should be inversely proportional to r_i. We design a simple but effective weighting factor and compute τ_i as below:

$$\tau_i = \frac{1}{\alpha r_i} \cdot \tau \tag{1}$$

where α is a hyper-parameter. For each lesion g_i, the proposals with an IoU greater than or equal to the threshold τ_i are selected as positive samples. The labeled proposals are then used to train the network.

2.2 Geometry-Adaptive RoI Fusion

RoIAlign maps each proposal to a single feature pyramid level, which fails to leverage multi-scale information from other levels. Some works [6,14] have attempted to integrate RoI features, but they do not consider the geometric characteristics of PAS bounding boxes. Hence, we design a GA-RF module to embed geometry prior into the representations of proposals. Given a proposal, the mapped RoI features $\{f_i^l \in \mathbb{R}^{c\times h\times w}\}_{l=1}^{L}$ in different levels are concatenated in channel dimension, where L is the number of levels. We define the proposal whose aspect ratio is greater than R as a hard sample. The number of hard samples distributed to each level is formulated as geometry prior knowledge $s_i \in \mathbb{R}^{1\times 4}$, which is used to generate fusion factor $\omega \in \mathbb{R}^{1\times 4}$. The fused feature $f_i \in \mathbb{R}^{cL\times h\times w}$ is the weighted sum of all feature levels and expressed as follows:

$$N_l = \sum\nolimits_{p\in P_l} \mathbb{I}(r_p \geq R),\ \omega = sigmoid(N_1, N_2, \cdots, N_L),\ f_i = \sum_{l=1}^{L} \omega_l \cdot f_i^l \tag{2}$$

where $\{N_l\}_{l=1}^{L}$ is the number of proposals with large aspect ratio in each layer. In this way, we take full advantage of the multi-scale information and the geometry distribution prior to enrich the feature representation for PAS prediction.

2.3 Lesion-Aware Detection Head

Motivated by [2,25], we present a Lesion-aware Detection Head (LA-Head) to use high-quality proposals to iteratively refine the lesion box labels.

In this work, we regard PAS detection as a multiple instance learning (MIL) problem. In the standard paradigm for object detection, a MIL method treats an image as a bag and proposals in the image as instances [13,28]. Different from previous studies, we treat an object as a bag B_i and proposals corresponding to the object as instances $P_i = \{p_i^j\}_{j=1}^{N}$, where N is the number of instances. Each bag has a label $y_i \in \{1, -1\}$, where $y_i = 1$ denotes an inaccurate ground-truth box containing at least one lesion candidate and $y_i = -1$ denotes a background box without lesions.

As shown in Fig. 1(c), our lesion-aware MIL method can be separated into three alternative parts: detector $\mu(\theta^d)$, instance selector $\phi(\theta^s)$ and instance classifier $\psi(\theta^c)$, where θ^d, θ^s and θ^c are parameters to be learned. First, the detector

generates lesion instances based on proposal features. Then for each instance p_i^j, the instance selector computes the confidence score $\phi(p_i^j;\theta^s)$. Considering that the classification scores are not strongly correlated with localization quality [11], we select the most positive instance $p_i^{j^*}$ as follows:

$$j^* = \arg\max_j \phi(p_i^j;\theta^s) \tag{3}$$

where j^* is the index of the instance with the highest score. To leverage the classification information of predicted bounding boxes, we fuse the most positive instance $p_i^{j^*}$ and the ground-truth instance g_i to obtain a high-quality positive instance for training. The final selected instance is defined as below:

$$p_i^* = \delta_s(\phi(p_i^{j^*};\theta^s)) \cdot p_i^{j^*} + (1 - \delta_s(\phi(p_i^{j^*};\theta^s))) \cdot g_i \tag{4}$$

where δ_s is the weighting factor. Intuitively, the weight assigned to p_i^* should be higher when $\phi(p_i^{j^*};\theta^s)$ is larger, and the weight assigned to g_i should have a lower bound γ to ensure that g_i can provide prior knowledge. Thus δ_s is calculated as:

$$\delta_s(x) = \min(e^{\beta \cdot x}, \gamma) \tag{5}$$

where β and γ are hyper-parameters. With the selected instances, instance classifier is trained to classify other instances as positive or negative. Then these proposals can serve as refined bounding box annotations for the detector. Furthermore, the detector generates instances to train the detection head and high-quality proposals can improve the detection performance. Thus this enables the self-feedback relationship between the detector and the LA-Head.

During training, instance selector, instance classifier and detector are jointly optimized based on the loss function:

$$L = \sum\nolimits_i (L_s(B_i, \varphi(\theta^s)) + L_c(B_i, p_i^*, \phi(\theta^c)) + L_d(B_i, p_i^*, \mu(\theta^d)) \tag{6}$$

where L_s is the loss of instance selector which is defined as hinge loss:

$$L_s(B_i, \phi(\theta^c)) = \max(0, 1 - y_i \max_j \phi(p_i^j;\theta^c)) \tag{7}$$

The second term L_c is the loss of instance classifier and denoted as follows:

$$L_c(B_i, p_i^*, \psi(\theta^c)) = \sum\nolimits_j \log(y_i^j \cdot (\psi(p_i^j;\theta^c) - \frac{1}{2}) + \frac{1}{2}) \tag{8}$$

where $\psi(p_i^j;\theta^c)$ is the probability that p_i^j contains lesions, and y_i^j is the label of p_i^j and calculated as follows:

$$y_i^j = \begin{cases} 1, y_i = 1 \; and \; IoU(p_i^j, p_i^*) \geq \tau_i^* \\ -1, y_i = 1 \; and \; IoU(p_i^j, p_i^*) < \tau_i^* \\ -1, y_i = -1 \end{cases} \tag{9}$$

where τ_i^* is the dynamic IoU threshold of p_i^j. The third term L_d is defined as:

$$L_d(B_i, p_i^*, \mu(\theta^d)) = \sum_j \mathbb{1}(y_i) \cdot \mathbb{1}(y_i^j) \cdot L_{reg}(p_i^j, p_i^*) \tag{10}$$

where $\mathbb{1}(x)$ is the indicator function, set to 1 if $x = 1$; otherwise, set to 0. We adopt the smooth L_1 loss as the loss function L_{reg} for regression.

3 Experiments and Results

3.1 Dataset, Evaluation Metrics and Implementation Details

Dataset. Owing to the lack of open-source PAS dataset, our experiments are performed on a private dataset. We collected 110 placenta MRI scans of different patients upon the approval of Xiangya Hospital of Central South University. All T2-weighted image volumes were sliced along the sagittal plane. Two experienced radiologists with 20 and 14 years of clinical experience in medical imaging and PAS diagnosis selected the slices with PAS and manually annotated the lesion bounding boxes using LabelImg [24]. We finally obtain 312 2D MR images with a resolution of 640×640 px. To verify the robustness of our network, we simulate inaccurate annotations by perturbing clean bounding box labels. With the noise rate λ, we randomly shift and scale the ground-truth box $\{x_i, y_i, w_i, h_i\}$ as follows:

$$x_i^{'} = x_i + \Delta_x w_i, y_i^{'} = y_i + \Delta_y h_i, w_i^{'} = w_i + \Delta_w w_i, h_i^{'} = h_i + \Delta_h h_i \tag{11}$$

where Δx, Δy, Δw, and Δh follow the uniform distribution $U(-\lambda, \lambda)$.

Evaluation Metrics. We adopt Average Precision (AP) and Sensitivity to evaluate the detection performance. In detail, AP is calculated over IoU threshold ranges from 0.25 to 0.95 at an interval of 0.05. Sensitivity denotes the proportion of correct prediction results in all ground-truths and is computed with an IoU threshold of 0.25 at 1 false positive per image.

Implementation Details. The proposed network is implemented with MMDetection 2.4.0 [4] and Pytorch 1.6 on NVIDIA GeForce RTX 1080Ti. We took FPN with ResNet50 [8] as backbone. The framework was trained using the SGD optimizer, where the initial learning rate, momentum, and weight decay were $5e-4$, 0.9, and $1e-3$, respectively. We adopt a batch size of 1 and the epochs of 120. The hyper-parameters are set as $\alpha = 2$, $\beta = 0.2$, $\gamma = 0.8$ and $R = 2$.

3.2 Ablation Study

The results of ablative experiments are listed in Table 1. Faster R-CNN is set as the baseline. We first explore the impact of GA-LA and GA-RF under accurate annotations. Compared with the baseline, two components bring 3.4% and

Table 1. Ablation study of the proposed method.

GA-LA	GA-RF	LA-Head	AP_{25}	AP_{50}	mAP	Sensitivity
Data with clean labels						
×	×	×	65.1	35.6	25.4	79.5
✓	×	×	68.7	41.8	28.8 (+3.4)	90.4 (+10.9)
×	✓	×	68.9	47.7	30.4 (+5.0)	82.2 (+2.7)
✓	✓	×	**79.2**	**51.1**	**34.1(+8.7)**	**91.8(+12.3)**
Data with noisy labels ($\lambda = 0.1$)						
×	×	×	65.2	30.2	24.2	83.6
×	×	✓	69.5	30.9	26.4 (+2.2)	84.9 (+1.3)
✓	✓	✓	**74.0**	**40.4**	**30.3(+6.1)**	**86.3(+2.7)**
Data with noisy labels ($\lambda = 0.2$)						
×	×	×	60.2	25.9	21.0	78.1
×	×	✓	61.4	34.3	22.3 (+1.3)	80.8 (+2.7)
✓	✓	✓	**71.1**	**39.5**	**27.3(+6.3)**	**83.6(+5.5)**

5.0% mAP gains separately. Another 3.7% mAP improvement is achieved when applied together. This finding indicates that geometry information of lesions can behave as effective prior for PAS detection. We then add LA-Head and conduct experiments under inaccurate annotations. It outperforms the baseline by at least 1.3% mAP, which demonstrates that the classification information of predictions is beneficial to alleviate the impact of noisy bounding box labels. We subsequently combine all key designs and obtain the optimal 30.3% and 26.8% mAP under 10% and 20% noise levels, outperforming the baseline by 6.1% and 5.8% respectively. The results reveal that high-quality predictions with geometry guidance can provide precise supervision for LA-Head. In addition, our method brings more obvious improvement under high annotation noise, which further proves its robustness to inaccurate annotations.

3.3 Comparison with State-of-the-Art Methods

We compare the geometry-adaptive network with seven object detection methods on both clean and noisy datasets. Faster R-CNN, Cascade R-CNN [3] and Dynamic R-CNN [30] are anchor-based methods, while FCOS is an anchor-free detector. ATSS [31] and SA-S [9] are dynamic label assignment strategies. Note that SA-S also uses the object shape information to select samples. AugFPN [6] is a variant of FPN and contains a soft RoI selection module.

The quantitative results are reported in Table 2. We first analyze the results of experiments under clean data. Compared with the general anchor-based and anchor-free methods, our method outperforms them by a large margin, thereby verifying that higher-quality predictions are generated under the guidance of geometry information. Compared with dynamic label assignment strategies, the

Table 2. Comparison with state-of-the-art methods.

Methods	Data with clean labels				Data with noisy labels			
	AP_{25}	AP_{50}	mAP	Sensitivity	AP_{25}	AP_{50}	mAP	Sensitivity
Faster R-CNN [19]	65.1	35.6	25.4	79.5	65.2	30.2	24.2	83.6
Cascade R-CNN [3]	62.6	38.7	27.2	76.7	57.0	30.1	22.7	79.5
Dynamic R-CNN [30]	71.5	40.2	30.3	89.0	69.2	39.8	28.3	84.9
FCOS [23]	70.8	36.0	27.4	86.3	68.9	38.7	26.6	90.4
ATSS [31]	68.3	40.1	28.2	82.2	65.1	28.5	23.8	90.4
SA-S [9]	71.3	46.1	31.5	90.4	66.4	33.9	26.0	**91.8**
AugFPN [6]	70.7	40.1	29.0	87.8	59.1	36.1	24.0	79.5
Ours	**79.2**	**51.1**	**34.1**	**91.8**	**74.0**	**40.4**	**30.3**	86.3

improvement of mAP by 5.9%, 2.6% and sensitivity by 9.6%, 1.4% demonstrated that our GA-LA strategy is simple but effective. Although SA-S also considers the shape of objects, the proposed method still achieves superior performance, likely because our model benefits from the two-stage structure. Compared with the feature fusion method, our approach performs favorably against heuristic-guided RoI selection of AugFPN. An intuitive explanation is that the optimal feature may be difficult to obtain using heuristic-guided method. Meanwhile our GA-RF module can adaptively generate representation according to the geometry prior of PAS lesions. We then analyze experimental results under 10% noise level data. Our geometry-adaptive network achieves consistent performance improvements compared with other state-of-the-art detectors. The result reveals that the high-quality predictions can serve as precise supervision signals for learning on inaccurate annotations. Figure 2 provides the visualization results of Faster R-CNN, Dynamic R-CNN, SA-S and AugFPN. The examples show that our method can generate PAS bounding boxes with more accurate shape and localization, which is consistent with the previous analysis.

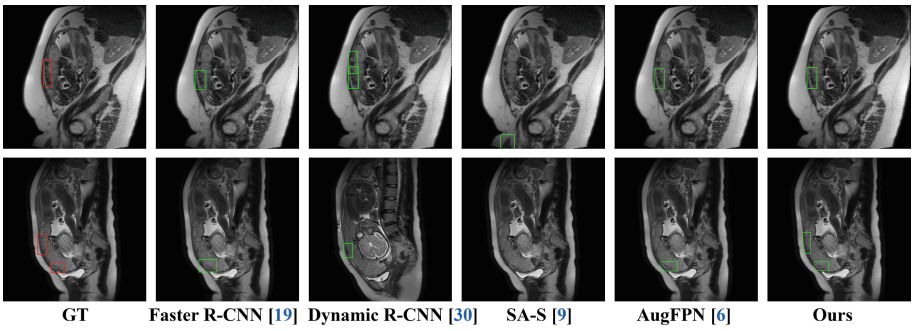

Fig. 2. Visualization of the detection results. Red bounding boxes represent the ground-truth while green bounding boxes represent predictions. The first row and second row are the results under clean and noisy labels respectively. (Color figure online)

4 Conclusion

In this paper, we present a geometry-adaptive network for robust PAS detection. We point out that the geometry prior missing problem and inaccurate annotations could deteriorate the performance of detectors. To solve the problem, a Geometry-adaptive Label Assignment strategy (GA-LA) and a Geometry-adaptive RoI Fusion (GA-RF) module are proposed to fully utilize the geometry prior of lesions to predict high-quality proposals. Moreover, a Lesion-aware Detection Head (LA-Head) is developed to alleviate the impact of inaccurate annotations by leveraging the classification information of predicted boxes. The experimental results under both clean and noisy labels demonstrate that our method surpasses other state-of-the-art detectors.

Acknowledgements. This work was supported by the National Natural Science Foundation of China (No. 61972419), and the Natural Science Foundation of Hunan Province, China (No. 2021JJ30865 and 2023JJ30865).

References

1. Baughman, W.C., Corteville, J.E., Shah, R.R.: Placenta accreta: spectrum of us and MR imaging findings. Radiographics **28**(7), 1905–1916 (2008)
2. Bilen, H., Vedaldi, A.: Weakly supervised deep detection networks. In: Proceedings of the IEEE Conference on Computer Vision and Pattern Recognition, pp. 2846–2854 (2016)
3. Cai, Z., Vasconcelos, N.: Cascade R-CNN: delving into high quality object detection. In: Proceedings of the IEEE Conference on Computer Vision and Pattern Recognition, pp. 6154–6162 (2018)
4. Chen, K., et al.: Mmdetection: open mmlab detection toolbox and benchmark. arXiv preprint arXiv:1906.07155 (2019)
5. El Gelany, S., et al.: Placenta accreta spectrum (PAS) disorders: incidence, risk factors and outcomes of different management strategies in a tertiary referral hospital in Minia, Egypt: a prospective study. BMC Pregnancy Childbirth **19**, 1–8 (2019)
6. Guo, C., Fan, B., Zhang, Q., Xiang, S., Pan, C.: AugFPN: improving multi-scale feature learning for object detection. In: Proceedings of the IEEE/CVF Conference on Computer Vision and Pattern Recognition, pp. 12595–12604 (2020)
7. He, K., Gkioxari, G., Dollár, P., Girshick, R.: Mask R-CNN. In: Proceedings of the IEEE International Conference on Computer Vision, pp. 2961–2969 (2017)
8. He, K., Zhang, X., Ren, S., Sun, J.: Deep residual learning for image recognition. In: Proceedings of the IEEE Conference on Computer Vision and Pattern Recognition, pp. 770–778 (2016)
9. Hou, L., Lu, K., Xue, J., Li, Y.: Shape-adaptive selection and measurement for oriented object detection. In: Proceedings of the AAAI Conference on Artificial Intelligence, vol. 36, pp. 923–932 (2022)
10. Jauniaux, E., Chantraine, F., Silver, R., Langhoff-Roos, J.: Figo placenta accreta diagnosis and management expert consensus panel. figo consensus guidelines on placenta accreta spectrum disorders: epidemiology. Int. J. Gynaecol. Obstet. **140**(3), 265–273 (2018)

11. Jiang, B., Luo, R., Mao, J., Xiao, T., Jiang, Y.: Acquisition of localization confidence for accurate object detection. In: Proceedings of the European Conference on Computer Vision (ECCV), pp. 784–799 (2018)
12. Lin, T.Y., Dollár, P., Girshick, R., He, K., Hariharan, B., Belongie, S.: Feature pyramid networks for object detection. In: Proceedings of the IEEE Conference on Computer Vision and Pattern Recognition, pp. 2117–2125 (2017)
13. Liu, C., Wang, K., Lu, H., Cao, Z., Zhang, Z.: Robust object detection with inaccurate bounding boxes. In: Avidan, S., Brostow, G., Cissé, M., Farinella, G.M., Hassner, T. (eds.) European Conference on Computer Vision. LNCS, vol. 13670, pp. 53–69. Springer, Cham (2022). https://doi.org/10.1007/978-3-031-20080-9_4
14. Liu, S., Qi, L., Qin, H., Shi, J., Jia, J.: Path aggregation network for instance segmentation. In: Proceedings of the IEEE Conference on Computer Vision and Pattern Recognition, pp. 8759–8768 (2018)
15. Masselli, G., et al.: Magnetic resonance imaging in the evaluation of placental adhesive disorders: correlation with color doppler ultrasound. Eur. Radiol. **18**, 1292–1299 (2008)
16. Mathai, T.S., et al.: Detection of lymph nodes in T2 MRI using neural network ensembles. In: Lian, C., Cao, X., Rekik, I., Xu, X., Yan, P. (eds.) MLMI 2021. LNCS, vol. 12966, pp. 682–691. Springer, Cham (2021). https://doi.org/10.1007/978-3-030-87589-3_70
17. Qi, H.: Prenatal assessment of placenta accreta spectrum disorders from ultrasound images using deep learning. Ph.D. thesis, University of Oxford (2019)
18. Qi, H., Collins, S., Noble, J.A.: Knowledge-guided pretext learning for uteroplacental interface detection. In: Martel, A.L., et al. (eds.) MICCAI 2020. LNCS, vol. 12261, pp. 582–593. Springer, Cham (2020). https://doi.org/10.1007/978-3-030-59710-8_57
19. Ren, S., He, K., Girshick, R., Sun, J.: Faster R-CNN: towards real-time object detection with region proposal networks. In: Advances in Neural Information Processing Systems, vol. 28 (2015)
20. Shao, Q., et al.: Deep learning and radiomics analysis for prediction of placenta invasion based on T2WI. Math. Biosci. Eng. **18**(5), 6198–6215 (2021)
21. Silver, R.M., Branch, D.W.: Placenta accreta spectrum. N. Engl. J. Med. **378**(16), 1529–1536 (2018)
22. Swinburne, N.C., et al.: Semisupervised training of a brain MRI tumor detection model using mined annotations. Radiology **303**(1), 80–89 (2022)
23. Tian, Z., Shen, C., Chen, H., He, T.: FCOS: fully convolutional one-stage object detection. In: Proceedings of the IEEE/CVF International Conference on Computer Vision, pp. 9627–9636 (2019)
24. Tzutalin: Labelimg (2015). https://github.com/heartexlabs/labelImg
25. Wan, F., Liu, C., Ke, W., Ji, X., Jiao, J., Ye, Q.: C-mil: continuation multiple instance learning for weakly supervised object detection. In: Proceedings of the IEEE/CVF Conference on Computer Vision and Pattern Recognition, pp. 2199–2208 (2019)
26. Wan, Z., Chen, Y., Deng, S., Chen, K., Yao, C., Luo, J.: Slender object detection: diagnoses and improvements. arXiv preprint arXiv:2011.08529 (2020)
27. Wang, S., et al.: Global-local attention network with multi-task uncertainty loss for abnormal lymph node detection in MR images. Med. Image Anal. **77**, 102345 (2022)
28. Xu, Y., Zhu, L., Yang, Y., Wu, F.: Training robust object detectors from noisy category labels and imprecise bounding boxes. IEEE Trans. Image Process. **30**, 5782–5792 (2021)

29. Xuan, R., Li, T., Wang, Y., Xu, J., Jin, W.: Prenatal prediction and typing of placental invasion using MRI deep and radiomic features. Biomed. Eng. Online **20**(1), 56 (2021)
30. Zhang, H., Chang, H., Ma, B., Wang, N., Chen, X.: Dynamic R-CNN: towards high quality object detection via dynamic training. In: Vedaldi, A., Bischof, H., Brox, T., Frahm, J.-M. (eds.) ECCV 2020. LNCS, vol. 12360, pp. 260–275. Springer, Cham (2020). https://doi.org/10.1007/978-3-030-58555-6_16
31. Zhang, S., Chi, C., Yao, Y., Lei, Z., Li, S.Z.: Bridging the gap between anchor-based and anchor-free detection via adaptive training sample selection. In: Proceedings of the IEEE/CVF Conference on Computer Vision and Pattern Recognition, pp. 9759–9768 (2020)

Clinical Applications – Breast